ARCHIVES OF ELECTRICAL ENGINEERING VOL. X(Y), pp. 1-19 (2026)

This paper has been accepted for publication in the AEE journal. This is the version, which has not been fully edited and content may change prior to final publication.
Citation information: DOI 10.24425/aee.2026.3545

Magnetic field modeling and performance analysis of an interior permanent magnet synchronous motor with stator auxiliary slots based on the exact subdomain method

YIXIANG ZHENG

School of Transportation and Vehicle Engineering, Shandong University of Technology
No.266, Xincun West Road, Zhangdian District, Zibo, Shandong Province, China
e-mail: 2761426883@qq.com

Abstract: Setting auxiliary slots in the stator teeth of an interior permanent magnet synchronous motor (IPMSM) can effectively improve the distribution of the main air gap magnetic field and reduce the cogging torque and torque ripple. However, the introduction of auxiliary slots increases the complexity of the main magnetic field distribution and makes modeling and analysis more difficult. This paper proposes a magnetic field modeling and analysis method for an IPMSM with stator slots based on the exact subdomain method. The stator auxiliary slot parameters are incorporated into the subdomain model, and based on the conservation principles of the electromagnetic parameters of the permanent magnet (PM) material, the interior V-type PM poles are equivalently transformed into U-type poles with regular boundaries, thereby effectively improving the magnetic field modeling accuracy of the stator slotted IPMSM. Comparative analysis using the finite-element method shows that the analytical results of the proposed model have high accuracy. After stator slotting, the cogging torque of the motor is significantly reduced, and the output performance is markedly improved. This research method provides a sound theoretical basis for the magnetic field analysis and electromagnetic design of motors with complex topological structures.

Key words: auxiliary slots, interior permanent magnet synchronous motor, no-load air gap magnetic field, subdomain analytical model

1. Introduction

The interior permanent magnet synchronous motor (IPMSM) is widely and extensively used in new energy vehicles, industrial automation, aerospace, and other related fields due to its significant advantages, such as high-power density, high efficiency, and strong flux-weakening capability [1–3]. Among them, the V-type IPMSM has the advantages of a relatively simple structure, high magnetic utilization, and strong mechanical safety. However, it still suffers from insufficient sinusoidality of the air gap flux density waveform, a high distortion rate, and relatively large cogging torque. Opening auxiliary slots in the stator can change the local magnetic circuit path, optimize the distribution of the air gap magnetic field, reduce the

This paper has been accepted for publication in the AEE journal. This is the version, which has not been fully edited and content may change prior to final publication.
Citation information: DOI 10.24425/aee.2026.3545

waveform distortion rate, and effectively weaken the cogging effect [4–6], which is an effective means of ameliorating the above issues.

Stator slotting affects the magnetic field distribution in the stator teeth as well as the permeance and flux density distributions in the main air gap, thereby leading to a more complex main magnetic circuit and making magnetic field analysis more difficult. At present, the finite-element method (FEM) is widely used for magnetic field modeling and analysis of stator slotted motors and for optimization analysis of slotting parameters. Although the FEM has high accuracy, it involves high modeling cost and long preprocessing time for complex topological structures [7]. Compared with the FEM, analytical methods offer the advantages of high computational speed, clear physical interpretation, and convenient parameter analysis and optimization. Therefore, it is important to develop an analytical model that can accurately characterize the magnetic-field behavior of complex topologies while maintaining high computational efficiency. Among existing magnetic-field analysis methods, the equivalent magnetic-circuit method is simple to implement and has a clear physical interpretation, but it is inadequate for describing complex slot geometries and air gap flux density harmonics [8]. The equivalent magnetic-network method can account for local magnetic saturation, but its modeling and iterative solution procedures are relatively complicated [9]. The conformal-mapping method can analyze slotting effects, but its analytical treatment becomes difficult when dealing with complex boundaries, such as interior V-type permanent magnets (PMs) and auxiliary slots [10]. In contrast, the subdomain method (SM) enables the efficient solution of complex motor magnetic fields through regional decomposition, analytical solution of the governing equations, and boundary-condition matching. It can accurately describe the complex magnetic-field distribution caused by slotted structures while maintaining high analytical efficiency [11].Many studies have been carried out by researchers at home and abroad on the application of the SM to the magnetic field solution of permanent magnet synchronous motors (PMSMs). Reference [12] established a relatively complete subdomain model for a surface-mounted permanent magnet synchronous motor (SPMSM), obtained the analytical expressions of the magnetic field in each region, and provided an analysis framework. Reference [13] took a high-speed SPMSM as the research object, realized fast magnetic field modeling, and analyzed the magnetic field distribution and basic electromagnetic performance of the motor. Reference [14] considered the influence of no-load leakage flux in the model calculation, thereby enhancing the engineering application value of the SM. With the continuous advancement of SM research, its applications have gradually expanded to the IPMSM and have been widely applied to the analysis of V-type IPMSM. Reference [15] established an analytical magnetic field model for a rotor-slotted surface-inset permanent magnet motor, while the simplification of the stator slot structure affects the accuracy of the model. Reference [16] established an analytical magnetic field model for a rotor-slotted IPMSM, however, the generality of the model is limited by structural assumptions and applicable conditions. Reference [17] applied the subdomain model to the IPMSM with a high saliency ratio, providing a clearer description of its electromagnetic characteristics. Reference [18] developed a model for a V-type IPMSM based on segmented magnetization modeling of PMs, providing a new analytical approach, although the model accuracy still

This paper has been accepted for publication in the AEE journal. This is the version, which has not been fully edited and content may change prior to final publication.
Citation information: DOI 10.24425/aee.2026.3545

requires improvement. Reference [19] constructed a subdomain model for an IPMSM through rotor reconstruction and magnetic flux equivalence, thereby reducing the difficulty of direct modeling. Reference [20] established an analytical model of the no-load air gap magnetic field for a V-type IPMSM, improving the solution accuracy of the model.

Current SMs for IPMSMs commonly approximate the interior PMs as surface-mounted magnetic poles. However, this equivalent treatment cannot adequately represent the actual geometric boundaries of the interior magnets or their local magnetic-field characteristics, thereby limiting the model accuracy. Moreover, existing SMs have paid relatively little attention to auxiliary slots in the stator of permanent-magnet motors, and their effects on the local air gap permeance and magnetic-field distribution have not been fully considered during modeling. Therefore, this paper proposes a subdomain analytical model for an IPMSM considering stator slotting, in which the stator auxiliary slot parameters are incorporated into the model, and the interior V-type PM poles are equivalently transformed into U-type poles with regular boundaries based on the conservation principles of the electromagnetic parameters of the PM material, thereby effectively improving the magnetic field modeling accuracy of the stator slotted IPMSM. The analytical expression of the main air gap flux density considering stator slotting is derived, and the FEM is used for comparative analysis and performance verification.

2. The analytical model

This paper takes a Toyota Prius V-type IPMSM as the research object. To optimize the air gap magnetic-field distribution, reduce the cogging torque, and facilitate the subsequent formulation and solution of the analytical model, sector-shaped auxiliary slots symmetric about the centerline of each stator tooth are introduced at the stator tooth tips. The basic performance parameters of the stator slotted IPMSM under study are listed in Table 1, and its structure is shown in Fig. 1.

Table 1. Parameters of V-type IPMSM

Parameters (unit)	**Value**	**Parameters (unit)**	**Value**
Number of pole pairs	4	Rated/peak power (kW)	30/50
Number of stator slots	48	Rated/peak torque (N·m)	191/400
Rated speed (r/min)	1500	Stator and rotor core material	M19_29G
Direct current bus voltage (V)	500	PM material	N36Z_20
Permanent-magnet span angle (°)	35	Rated frequency (HZ)	100
Auxiliary slot angular width (°)	2	Auxiliary slot depth (mm)	0.2
Angle between the auxiliary-slot centerline and the stator tooth centerline (°)	1	Air gap length (mm)	0.75
Permanent-magnet thickness (mm)	6.5	Permanent-magnet width (mm)	16

This paper has been accepted for publication in the AEE journal. This is the version, which has not been fully edited and content may change prior to final publication.
Citation information: DOI 10.24425/aee.2026.3545

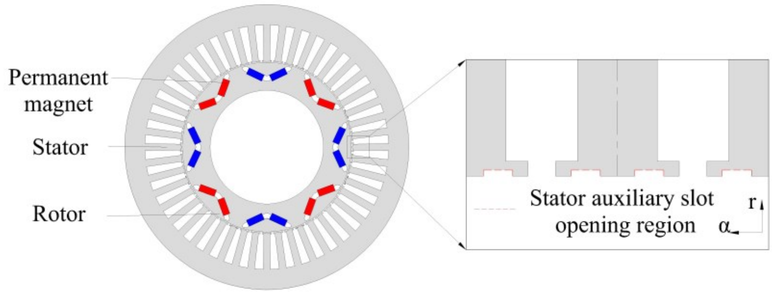

Fig. 1. Structure of the stator slotted IPMSM and schematic diagram of stator slotting

As can be seen from Fig. 1, the stator auxiliary slots are arranged on the inner side of the stator teeth, and auxiliary slots are introduced on both the left and right sides of each stator tooth. The two auxiliary slots are symmetrical about the radial centerline of the stator tooth.

2.1. Equivalent treatment of the rotor structure

To avoid complicated subdomain division and boundary condition treatment, the V-type PM structure is equivalently transformed into a radially magnetized structure and a tangentially magnetized structure [21–22], as shown in Fig. 2:

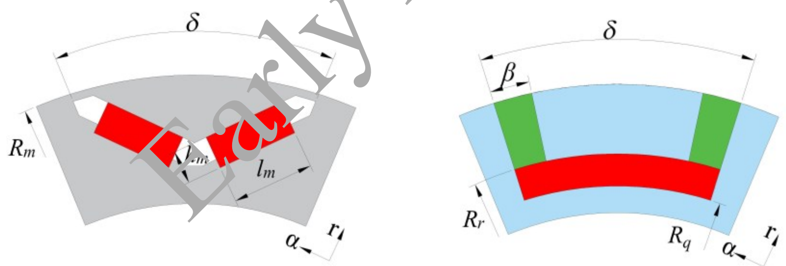

Fig. 2. Structure of the V-type IPMSM before equivalence (left) and after equivalence (right)

As can be seen from Fig. 2, the span angle of the PM remains unchanged. According to the principles of magnetic flux conservation and magnetomotive force conservation, the equivalent relationship satisfies the following equation:

$$\begin{cases} 2Brl_m = 2B_r^1 \ (R_m - R_r) + (\delta - 2\beta)B_r^1 R_r \\ \beta = \frac{Rr - Rq}{Rm} \\ h_m Br = 3B_r^1 (Rr - Rq) \end{cases}, \tag{1}$$

where: Br and B_r^1 are the remanent flux densities of PMs before and after equivalence, respectively, and the remanent flux densities of the equivalent radially magnetized and tangentially magnetized PMs are the same. R_r and R_q are the outer radius and inner radius of the

This paper has been accepted for publication in the AEE journal. This is the version, which has not been fully edited and content may change prior to final publication.
Citation information: DOI 10.24425/aee.2026.3545

equivalent radially magnetized PM, respectively, and β is the span angle of the equivalent radially magnetized PM. δ is the central angle occupied by the two PMs, h_m is the thickness of the V-type PM, l_m is the width of the V-type PM, and R_m is the outer diameter of the motor rotor.

The motor is divided into six subdomains: the tangentially magnetized permanent-magnet subdomain (Subdomain I), the radially magnetized permanent-magnet subdomain (Subdomain II), the air gap subdomain (Subdomain III), the sector auxiliary opening slot subdomain (Subdomain IV), the stator slot opening subdomain (Subdomain V), and the stator slot subdomain (Subdomain VI). The subdomain model of the equivalent permanent magnet motor is shown in Fig. 3.

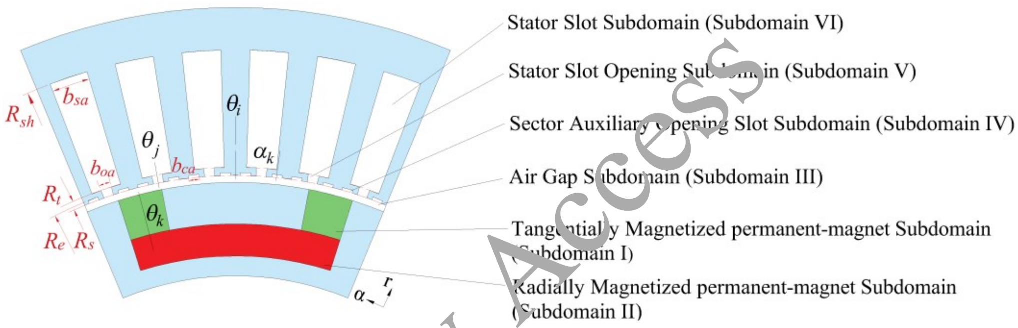

Fig. 3. Subdomain model of the equivalent permanent magnet motor

As can be seen from Fig. 3, θ_i and αk are the central angle of the stator slot opening and the central angle of the auxiliary slot opening, respectively. The angular position of the centerline of the k-th tangentially magnetized PM is defined as θ_k, and the installation central angle of the i-th V-type PM is defined as θ_i. R_{sh} is the radius of the stator slot bottom surface and R_t is the radius of the stator slot opening. R_s is the radius of the inner surface of the stator and R_e is the radius of the auxiliary slot bottom. bca is the slot width angle of the auxiliary slot. b_{sa} and b_{oa} are the stator slot width angle and the stator slot opening width angle, respectively.

To simplify the mathematical model, the following assumptions are made: the model is solved in a two-dimensional polar coordinate system; the eddy current effect and end effect are neglected; the demagnetization curve of the PM material is linear; the permeability of the stator and rotor cores is infinite; and the conductivity of the materials is 0 [23].

2.2. General solution of the tangentially magnetized permanent-magnet subdomain (Subdomain I)

In the two-dimensional polar coordinate system, magnetic field excitation exists in the tangentially magnetized permanent-magnet subdomain, and the vector magnetic potential is described by the Poisson equation as follows [24]:

This paper has been accepted for publication in the AEE journal. This is the version, which has not been fully edited and content may change prior to final publication.
Citation information: DOI 10.24425/aee.2026.3545

$$\begin{cases} \frac{\partial^2 A_{z\mathrm{I}}}{\partial r^2} + \frac{1}{r}\frac{\partial A_{z\mathrm{I}}}{\partial r} + \frac{1}{r^2}\frac{\partial^2 A_{z\mathrm{I}}}{\partial \alpha^2} = -\frac{\mu_0}{r}\left(M_{1\alpha} - \frac{\partial M_{1r}}{\partial \alpha}\right) \\ R_r < r < R_m, \theta_k - \frac{\beta}{2} < \alpha < \theta_k + \frac{\beta}{2} \end{cases}, \tag{2}$$

where: $M_{1\alpha}$ is the tangential component of the magnetization intensity of the PM, $M_{1\alpha} = 0$; M_{1r} is the radial component of the magnetization intensity of the PM, $M_{1r} = \frac{B_r^1}{\mu_0}$.

The boundary conditions are:

$$H_r^I\left(r, \theta_k \pm \frac{\beta}{2}\right) = 0, R_r < r < R_m. \tag{3}$$

By using the method of separation of variables, the general solution of the vector magnetic potential and the expression of the tangential magnetic field intensity in the tangentially magnetized permanent-magnet subdomain satisfying the boundary conditions can be obtained as:

$$A_{zI} = A_1^0 + B_1^0 \ln r - B_r^1 r + \sum_{n=1}^{\infty}\left[C_1^n \left(\frac{r}{R_m}\right)^{\frac{n\pi}{\beta}} + D_1^n \left(\frac{r}{R_r}\right)^{-\frac{n\pi}{\beta}}\right]\cos\left(\frac{n\pi}{\beta}\left(\alpha - \theta_k + \frac{\beta}{2}\right)\right), \tag{4}$$

$$H_{\alpha I} = \frac{-B_1^0}{\mu_0 \mu_r r} - \frac{1}{\mu_0 \mu_r}\sum_{n=1}^{\infty}\frac{n\pi}{\beta r}\left[C_1^n \left(\frac{r}{R_m}\right)^{\frac{n\pi}{\beta}} - D_1^n \left(\frac{r}{R_r}\right)^{-\frac{n\pi}{\beta}}\right]\cos\left(\frac{n\pi}{\beta}\left(\alpha - \theta_k + \frac{\beta}{2}\right)\right), \tag{5}$$

where: μ_0 is the permeability of vacuum, μ_r is the relative permeability of the PM, n is the harmonic order in the tangentially magnetized permanent-magnet subdomain, and the harmonic coefficients A_1^0, B_1^0, C_1^n, and D_1^n need to be solved according to the boundary conditions.

2.3. General solution of the radially magnetized permanent-magnet subdomain (Subdomain II)

Similarly, in the two-dimensional polar coordinate system, the vector magnetic potential in the radially magnetized permanent-magnet subdomain is described by the Poisson equation as follows:

$$\begin{cases} \frac{\partial^2 A_{z\mathrm{II}}}{\partial r^2} + \frac{1}{r}\frac{\partial A_{z\mathrm{II}}}{\partial r} + \frac{1}{r^2}\frac{\partial^2 A_{z\mathrm{II}}}{\partial \alpha^2} = -\frac{\mu_0}{r}\left(M_{2\alpha} - \frac{\partial M_{2r}}{\partial \alpha}\right) \\ R_q < r < R_r, \theta_i - \frac{\delta}{2} < \alpha < \theta_i + \frac{\delta}{2} \end{cases}, \tag{6}$$

where: $M_{2\alpha}^i$ is the tangential component of the magnetization intensity of the *i*-th radially magnetized permanent-magnet subdomain, $M_{2\alpha}^i = 0$; M_{2r}^i is the radial component of the magnetization intensity of the *i*-th radially magnetized permanent-magnet subdomain,

$$M_{2r}^i = (-1)^{i-1}\sum_{m=1}^{\infty} M_{2ru}^i \sin\left(F_m\left(\alpha - \theta_i + \frac{\delta}{2}\right)\right),$$

M_{2ru}^i is the magnetization intensity coefficient of the *i*-th radially magnetized PM and

$$M_{2ru}^i = \frac{4B_r^1}{m\pi\mu_0}\sin\left(\frac{m\pi}{2}\right)\sin\left(\frac{m\pi\alpha_1}{2\delta}\right).$$

This paper has been accepted for publication in the AEE journal. This is the version, which has not been fully edited and content may change prior to final publication.
Citation information: DOI 10.24425/aee.2026.3545

The boundary conditions are:

$$\begin{cases} H_r^{\mathrm{II}}\left(r, \theta_i \pm \frac{\delta}{2}\right) = 0, R_q < r < R_r \\ H_\alpha^{\mathrm{II}}(R_r, \alpha) = 0, \theta_i - \frac{\alpha_1}{2} < \alpha < \theta_i + \frac{\alpha_1}{2}, \\ H_\alpha^{\mathrm{II}}\left(R_q, \alpha\right) = 0, \theta_i - \frac{\delta}{2} < \alpha < \theta_i + \frac{\delta}{2} \end{cases} \tag{7}$$

By using the method of separation of variables, the general solution of the vector magnetic potential in the radially magnetized permanent-magnet subdomain satisfying the boundary conditions can be obtained as:

$$A_{z\mathrm{II}} = A_2^0 + \sum_{m=1}^{\infty} \left[C_2^m \left(\frac{r}{R_r}\right)^{\frac{m\pi}{\delta}} + D_2^m \left(\frac{r}{R_q}\right)^{-\frac{m\pi}{\delta}} + g_i(r) \right] \cos\left(\frac{m\pi}{\delta}\left(\alpha - \theta_i + \frac{\delta}{2}\right)\right), \tag{8}$$

where:

$$g_i(r) = (-1)^{i-1}\left(\frac{m\pi\delta\mu_0 r M_{2ru}^i}{m^2\pi^2 - \delta^2}\right), \tag{9}$$

$$D_2^m = C_2^m \left(\frac{R_r}{R_q}\right)^{-\frac{m\pi}{\delta}} + \frac{R_q g_i(R_q)}{F_m}. \tag{10}$$

The expression of the tangential magnetic field intensity in the radially magnetized permanent-magnet subdomain (Subdomain II) is:

$$H_{z\mathrm{II}} = \frac{-1}{\mu_r \mu_0} \sum_{m=1}^{\infty} \left[\frac{m\pi}{r\delta} C_2^m \left(\frac{r}{R_r}\right)^{\frac{m\pi}{\delta}} - \frac{m\pi}{r\delta} D_2^m \left(\frac{r}{R_q}\right)^{-\frac{m\pi}{\delta}} + g_i'(r) \right] \cos\left(\frac{m\pi}{\delta}\left(\alpha - \theta_i + \frac{\delta}{2}\right)\right), \tag{11}$$

$$g_i'(r) = (-1)^{i-1}\left(\frac{-m\pi\delta\mu_0 M_{2ru}^i}{m^2\pi^2 - \delta^2}\right), \tag{12}$$

where: m is the harmonic order in the radially magnetized permanent-magnet subdomain, and the harmonic coefficients A_2^0, C_2^m and D_2^m need to be solved according to the boundary conditions.

2.4. General solution of the air gap subdomain (Subdomain III)

In the air gap subdomain, the vector magnetic potential can be described by the Laplace equation as follows [25-26]:

$$\begin{cases} \frac{\partial^2 A_{z\mathrm{III}}}{\partial r^2} + \frac{1}{r}\frac{\partial A_{z\mathrm{III}}}{\partial r} + \frac{1}{r^2}\frac{\partial^2 A_{z\mathrm{III}}}{\partial \alpha^2} = 0 \\ R_m < r < R_s, 0 < \alpha < 2\pi \end{cases}. \tag{13}$$

When $r = R_s$, if α falls within the angular region of the auxiliary slot, the air gap subdomain is connected with Subdomain IV; if α falls within the angular region of the stator slot opening, the air gap subdomain is connected with Subdomain V; otherwise, it is a high-permeability boundary of the iron core, thus:

This paper has been accepted for publication in the AEE journal. This is the version, which has not been fully edited and content may change prior to final publication.
Citation information: DOI 10.24425/aee.2026.3545

$$\begin{cases} H_\alpha^{\mathrm{III}}(R_s,\alpha)=H_\alpha^{\mathrm{IV}}(R_s,\alpha), & \alpha_k-\frac{o}{2}<\alpha<\alpha_k+\frac{o}{2} \\ H_\alpha^{\mathrm{III}}(R_s,\alpha)=H_\alpha^{\mathrm{V}}(R_s,\alpha), & \theta_j-\frac{b_{oa}}{2}<\alpha<\theta_j+\frac{b_{oa}}{2} \\ H_\alpha^{\mathrm{III}}(R_s,\alpha)=0, & \text{elsewhere} \end{cases}. \tag{14}$$

Meanwhile, when $r=R_m$, if α falls within the angular region of the tangentially magnetized PM, the air gap subdomain is connected with Subdomain I; otherwise, the air gap subdomain is a high-permeability boundary of the iron core, thus:

$$\begin{cases} H_\alpha^{\mathrm{III}}(R_m,\alpha)=H_\alpha^{I}(R_m,\alpha), & \theta_k-\frac{\beta}{2}<\alpha<\theta_k+\frac{\beta}{2} \\ H_\alpha^{\mathrm{III}}(R_m,\alpha)=0, & \text{elsewhere} \end{cases}, \tag{15}$$

By using the method of separation of variables, the general solution of the vector magnetic potential and the expression of the tangential magnetic field intensity in the air gap subdomain satisfying the boundary conditions can be obtained as:

$$A_{z\mathrm{III}}=\sum_{v=1}^{\infty}\left[A_3^{v}\left(\frac{r}{R_s}\right)^{v}+B_3^{v}\left(\frac{r}{R_m}\right)^{-v}\right]\cos(v\alpha)+\sum_{v=1}^{\infty}\left[C_3^{v}\left(\frac{r}{R_s}\right)^{v}+D_3^{v}\left(\frac{r}{R_m}\right)^{-v}\right]\sin(v\alpha)+E_3^{0}, \tag{16}$$

$$H_{\alpha\mathrm{III}}=\frac{-1}{\mu_0}\sum_{v=1}^{\infty}\frac{v}{r}\left[A_3^{v}\left(\frac{r}{R_s}\right)^{v}-B_3^{v}\left(\frac{r}{R_m}\right)^{-v}\right]\cos(v\alpha)+\frac{-1}{\mu_0}\sum_{v=1}^{\infty}\frac{v}{r}\left[C_3^{v}\left(\frac{r}{R_s}\right)^{v}-D_3^{v}\left(\frac{r}{R_m}\right)^{-v}\right]\sin(v\alpha), \tag{17}$$

where: v is the harmonic order of the air gap subdomain, and A_3^v, B_3^v, C_3^v, D_3^v and E_3^0 are the harmonic coefficients of the air gap subdomain. At $r=R_m$, the air gap subdomain and the tangentially magnetized permanent-magnet subdomain satisfy the continuity conditions of Az and the tangential magnetic field intensity. And when $r=R_s$, the air gap subdomain and the sector auxiliary opening slot subdomain as well as the stator slot opening subdomain also satisfy the continuity conditions of Az and the tangential magnetic field intensity, respectively. Accordingly, the coefficients in the above general solution of the vector magnetic potential in the air gap subdomain can be further determined.

2.5. General solution of the sector auxiliary opening slot subdomain (Subdomain IV)

In the sector auxiliary opening slot subdomain, the vector magnetic potential can be described by the Laplace equation as follows:

$$\begin{cases} \frac{\partial^2 A_{z\mathrm{IV}}}{\partial r^2}+\frac{1}{r}\frac{\partial A_{z\mathrm{IV}}}{\partial r}+\frac{1}{r^2}\frac{\partial^2 A_{z\mathrm{IV}}}{\partial \alpha^2}=0 \\ R_s<r<R_e, \alpha_k-bca/2<\alpha<\alpha_k+bca/2 \end{cases}. \tag{18}$$

The boundary conditions are:

$$H_\alpha^{\mathrm{IV}}(R_e,\alpha)=0, 0<\alpha<2\pi. \tag{19}$$

By using the method of separation of variables, the general solution of the vector magnetic potential and the expression of the tangential magnetic field intensity in the sector auxiliary opening slot subdomain satisfying the boundary conditions can be obtained as:

This paper has been accepted for publication in the AEE journal. This is the version, which has not been fully edited and content may change prior to final publication.
Citation information: DOI 10.24425/aee.2026.3545

$$A_{z\mathrm{IV}} = A_4^0 + \sum_{\chi=1}^{\infty}\left[C_4^{\chi}\left(\frac{r}{R_e}\right)^{\frac{\chi\pi}{bca}} + D_4^{\chi}\left(\frac{r}{R_s}\right)^{-\frac{\chi\pi}{bca}}\right]\cos\left(\frac{\chi\pi}{bca}\left(\alpha-\alpha_k+\frac{bca}{2}\right)\right), \tag{20}$$

$$H_{\alpha\mathrm{IV}} = \frac{-1}{\mu_0}\sum_{\chi=1}^{\infty}\frac{\chi\pi}{rbca}\left[C_4^{\chi}\left(\frac{r}{R_e}\right)^{\frac{\chi\pi}{bca}} - D_4^{\chi}\left(\frac{r}{R_s}\right)^{-\frac{\chi\pi}{bca}}\right]\cos\left(\frac{\chi\pi}{bca}\left(\alpha-\alpha_k+\frac{bca}{2}\right)\right), \tag{21}$$

where: χ is the harmonic order of the sector auxiliary opening slot subdomain. A_4^0, C_4^{χ} and D_4^{χ} are the harmonic coefficients of this subdomain, which need to be solved according to the boundary conditions.

2.6. General solution of the stator slot opening subdomain (Subdomain V)

In the stator slot opening subdomain, the vector magnetic potential can be described by the Laplace equation as follows:

$$\begin{cases}\frac{\partial^2 A_{z\,\mathrm{V}}}{\partial r^2}+\frac{1}{r}\frac{\partial A_{z\,\mathrm{V}}}{\partial r}+\frac{1}{r^2}\frac{\partial^2 A_{z\,\mathrm{V}}}{\partial \alpha^2}=0\\ R_s<r<R_t, \theta_j-\frac{b_{oa}}{2}<\alpha<\theta_j+\frac{b_{oa}}{2}\end{cases} \tag{22}$$

The boundary conditions are:

$$H_r^{\mathrm{V}}\left(r,\theta_j\pm\frac{b_{oa}}{2}\right)=0, \quad R_s<r<R_t. \tag{23}$$

By using the method of separation of variables, the general solution of the vector magnetic potential and the expression of the tangential magnetic field intensity in the stator slot opening subdomain satisfying the boundary conditions can be obtained as:

$$A_{z\mathrm{V}} = A_5^0 + B_5^0\ln r + \sum_{k=1}^{\infty}\left[C_5^{k}\left(\frac{r}{R_t}\right)^{\frac{k\pi}{b_{oa}}} + D_5^{k}\left(\frac{r}{R_s}\right)^{-\frac{k\pi}{b_{oa}}}\right]\cos\left(\frac{k\pi}{b_{oa}}\left(\alpha-\theta_j+\frac{b_{oa}}{2}\right)\right), \tag{24}$$

$$H_{\alpha\mathrm{V}} = \frac{-B_5^0}{\mu_0 r} + \frac{-1}{\mu_0}\sum_{k=1}^{\infty}\frac{k\pi}{rboa}\left[C_5^{k}\left(\frac{r}{R_t}\right)^{\frac{k\pi}{b_{oa}}} - D_5^{k}\left(\frac{r}{R_s}\right)^{-\frac{k\pi}{b_{oa}}}\right]\cos\left(\frac{k\pi}{b_{oa}}\left(\alpha-\theta_j+\frac{b_{oa}}{2}\right)\right), \tag{25}$$

where: k is the harmonic order of the stator slot opening subdomain, A_5^0, B_5^0, C_5^k and D_5^k are the harmonic coefficients of the stator slot opening subdomain and need to be solved according to the boundary conditions.

2.7. General solution of the stator slot subdomain (Subdomain VI)

In the stator slot subdomain, the vector magnetic potential can be described by the Laplace equation as follows:

$$\begin{cases}\frac{\partial^2 A_{z\mathrm{VI}}}{\partial r^2}+\frac{1}{r}\frac{\partial A_{z\mathrm{VI}}}{\partial r}+\frac{1}{r^2}\frac{\partial^2 A_{z\mathrm{VI}}}{\partial \alpha^2}=0\\ R_t<r<R_{sh}, \theta_j-\frac{b_{sa}}{2}<\alpha<\theta_j+\frac{b_{sa}}{2}\end{cases}. \tag{26}$$

The boundary conditions are:

This paper has been accepted for publication in the AEE journal. This is the version, which has not been fully edited and content may change prior to final publication.
Citation information: DOI 10.24425/aee.2026.3545

$$H_{\alpha}^{\mathrm{VI}}(R_{sh},\alpha)=0,\quad 0<\alpha<2\pi. \tag{27}$$

By using the method of separation of variables, the general solution of the vector magnetic potential and the expression of the tangential magnetic field intensity in the stator slot subdomain satisfying the boundary conditions can be obtained as:

$$A_{z\mathrm{VI}}=A_6^0+\sum_{\gamma=1}^{\infty}B_6^{\gamma}\left[\left(\frac{R_t}{R_{sh}}\right)^{\frac{\gamma\pi}{b_{sa}}}\left(\frac{r}{R_{sh}}\right)^{\frac{\gamma\pi}{b_{sa}}}+\left(\frac{r}{R_t}\right)^{-\frac{\gamma\pi}{b_{sa}}}\right]\cos\left(\frac{\gamma\pi}{b_{sa}}\left(\alpha-\theta_j+\frac{b_{sa}}{2}\right)\right), \tag{28}$$

$$H_{\alpha\mathrm{VI}}=\frac{-1}{\mu_0}\sum_{\gamma=1}^{\infty}B_6^{\gamma}\frac{F_{\gamma}}{r}\left[\left(\frac{R_t}{R_{sh}}\right)^{\frac{\gamma\pi}{b_{sa}}}\left(\frac{r}{R_{sh}}\right)^{\frac{\gamma\pi}{b_{sa}}}-\left(\frac{r}{R_t}\right)^{-\frac{\gamma\pi}{b_{sa}}}\right]\cos\left(\frac{\gamma\pi}{b_{sa}}\left(\alpha-\theta_j+\frac{b_{sa}}{2}\right)\right), \tag{29}$$

where: γ is the harmonic order of the stator slot subdomain, and A_6^0, B_6^{γ} are the harmonic coefficients of the stator slot subdomain, and need to be solved according to the boundary conditions.

3. Solution of the harmonic coefficients

According to the analytical solutions of each subdomain, the continuity condition of the vector magnetic potential and the continuity condition of the tangential magnetic field intensity are imposed at the interfaces between adjacent subdomains, and the undetermined coefficients in each subdomain are solved simultaneously [27–28].

3.1. Interface between Subdomain I and Subdomain II

At the interface between the tangentially magnetized permanent-magnet subdomain and the radially magnetized permanent-magnet subdomain, that is, at $r=R_r$, according to the boundary conditions of the static magnetic field, the vector magnetic potential is continuous across the interface, and the tangential magnetic field intensity is continuous:

$$A_{z\mathrm{I}}|_{r=R_r}-A_{z\mathrm{II}}|_{r=R_r}=0,\theta_k-\frac{\beta}{2}\le\alpha\le\theta_k+\frac{\beta}{2}, \tag{30}$$

$$H_{\alpha\mathrm{I}}|_{r=R_r}-H_{\alpha\mathrm{II}}|_{r=R_r}=0,\theta_k-\frac{\beta}{2}\le\alpha\le\theta_k+\frac{\beta}{2}. \tag{31}$$

After substituting the expressions of the tangential magnetic field intensity of the two subdomains, Eq. (5) and Eq. (11), into Eq. (31), and unifying the tangential component of the magnetic field intensity in the tangentially magnetized permanent-magnet subdomain (Subdomain I) to the interval $\left[\theta_i-\frac{\delta}{2}\ \theta_i+\frac{\delta}{2}\right]$ by Fourier transform, the following can be obtained:

$$\begin{cases} \frac{2}{\delta}\int_{\theta_i-\frac{\delta}{2}}^{\theta_i+\frac{\delta}{2}} H_{\alpha\mathrm{I}}(R_r,\alpha)\cos\left(\frac{m\pi}{\delta}\left(\alpha-\theta_i+\frac{\delta}{2}\right)\right)\mathrm{d}\alpha = \\ \frac{-m\pi C_2^m}{\delta\mu_0\mu_r R_r} + \frac{m\pi C_2^m (R_q)^{\frac{2m\pi}{\delta}}}{\delta\mu_0\mu_r R_r^{\left(\frac{2m\pi}{\delta}+1\right)}} + \frac{R_q^{\left(\frac{m\pi}{\delta}+1\right)} g_i'(R_q)}{\mu_0\mu_r R_q^{\left(\frac{m\pi}{\delta}+1\right)}} - \frac{g_i'(R_r)}{\mu_0\mu_r} \\ \frac{1}{\delta}\int_{\theta_i-\frac{\delta}{2}}^{\theta_i+\frac{\delta}{2}} H_{\alpha\mathrm{I}}(R_r,\alpha)\mathrm{d}\alpha \end{cases}. \tag{32}$$

After substituting the expressions of the vector magnetic potential of the two subdomains, Eq. (4) and Eq. (8), into Eq. (30), and expanding the vector magnetic potential of the radially magnetized permanent-magnet subdomain (Subdomain II) along the tangentially magnetized permanent-magnet subdomain (Subdomain I) by Fourier series, the following can be obtained:

$$\begin{cases} \frac{2}{\beta}\int_{\theta_k-\frac{\beta}{2}}^{\theta_k+\frac{\beta}{2}} A_{z\mathrm{II}}(R_r,\alpha)\cos\left(\frac{n\pi}{\beta}\left(\alpha-\theta_k+\frac{\beta}{2}\right)\right)\mathrm{d}\alpha = C_1^n\left(\frac{R_r}{R_m}\right)^{\frac{n\pi}{\beta}} + D_1^n \\ \frac{1}{\beta}\int_{\theta_k-\frac{\beta}{2}}^{\theta_k+\frac{\beta}{2}} A_{z\mathrm{II}}(R_r,\alpha)\mathrm{d}\alpha = A_1^0 + B_1^0 \ln R_r - D_r R_r \end{cases}. \tag{33}$$

3.2. Interface between Subdomain I and Subdomain III

At the interface between the tangentially magnetized permanent-magnet subdomain and the air gap subdomain, that is, at the outer surface radius of the rotor, namely at $r = R_m$, according to the boundary conditions of the static magnetic field, the vector magnetic potential is continuous across the interface, and the tangential magnetic field intensity is continuous:

$$A_{z\mathrm{I}}|_{r=R_m} - A_{z\mathrm{III}}|_{r=R_m} = 0,\ \ \theta_k - \frac{\beta}{2} \le \alpha \le \theta_k + \frac{\beta}{2}, \tag{34}$$

$$H_{\alpha\mathrm{I}}|_{r=R_m} - H_{\alpha\mathrm{III}}|_{r=R_m} = 0,\ \ \theta_k - \frac{\beta}{2} \le \alpha \le \theta_k + \frac{\beta}{2}. \tag{35}$$

After substituting the expressions of the tangential magnetic field intensity of the two subdomains, Eq. (5) and Eq. (17), into Eq. (35), and unifying the tangential component of the magnetic field intensity in the tangentially magnetized permanent-magnet subdomain (Subdomain I) to the interval $[0, 2\pi]$ by Fourier transform, the following can be obtained:

$$\begin{cases} \frac{1}{\pi}\int_{\theta_k-\frac{\beta}{2}}^{\theta_k+\frac{\beta}{2}} H_{\alpha\mathrm{I}}(R_m,\alpha)\cos(v\alpha)\mathrm{d}\alpha = \frac{-v}{\mu_0 R_m}\left(A_3^v\left(\frac{R_m}{R_s}\right)^v\right) - B_3^v \\ \frac{1}{\pi}\int_{\theta_k-\frac{\beta}{2}}^{\theta_k+\frac{\beta}{2}} H_{\alpha\mathrm{I}}(R_r,\alpha)\sin(v\alpha)\,\mathrm{d}\alpha = \frac{-v}{\mu_0 R_m}\left(C_3^v\left(\frac{R_m}{R_3}\right)^v\right) - D_3^v \end{cases}. \tag{36}$$

After substituting the expressions of the vector magnetic potential of the two subdomains, Eq. (4) and Eq. (16), into Eq. (34), and expanding the vector magnetic potential of the air gap

This paper has been accepted for publication in the AEE journal. This is the version, which has not been fully edited and content may change prior to final publication.
Citation information: DOI 10.24425/aee.2026.3545

subdomain(Subdomain III) along the tangentially magnetized permanent-magnet subdomain (Subdomain I) by Fourier series, the following can be obtained:

$$\begin{cases} \frac{2}{\beta}\int_{\theta_k-\frac{\beta}{2}}^{\theta_k+\frac{\beta}{2}} A_{z\mathrm{III}}(R_m,\alpha)\cos\left(\lambda_n\left(\alpha-\theta_k+\frac{\beta}{2}\right)\right)\mathrm{d}\alpha = C_1^n + D_1^n\left(\frac{R_m}{R_r}\right)^{-\frac{n\pi}{\beta}} \\ \frac{1}{\beta}\int_{\theta_k-\frac{\beta}{2}}^{\theta_k+\frac{\beta}{2}} A_{z\mathrm{III}}(R_m,\alpha)\mathrm{d}\alpha = A_1^0 + B_1^0\ln R_m - B_r^1 R_m \end{cases}. \tag{37}$$

3.3. Interface between Subdomain III and Subdomain IV

At the interface between the air gap subdomain and the sector auxiliary opening slot subdomain, that is, at the radius of the inner surface of the stator, namely at $r = R_s$. Similarly, the vector magnetic potential is continuous across the interface, and the tangential magnetic field intensity is continuous:

$$A_{z\mathrm{IV}}|_{r=R_s} - A_{z\mathrm{III}}|_{r=R_s} = 0, \alpha_k - \frac{bca}{2} \le \alpha \le \alpha_k + \frac{bca}{2}, \tag{38}$$

$$H_{\alpha\mathrm{IV}}|_{r=R_s} - H_{\alpha\mathrm{IIII}}|_{r=R_s} = 0, \alpha_k - \frac{bca}{2} \le \alpha \le \alpha_k + \frac{bca}{2}. \tag{39}$$

After substituting the expressions of the tangential magnetic field intensity of the two subdomains, Eq. (17) and Eq. (21), into Eq. (39), and unifying the tangential component of the magnetic field intensity in the sector auxiliary opening slot subdomain (Subdomain IV) to the interval $[0,2\pi]$ by Fourier transform, the following can be obtained:

$$\begin{cases} \frac{1}{\pi}\int_{\alpha_k-\frac{bc\alpha}{2}}^{\alpha_k+\frac{bc\alpha}{2}} H_{\alpha\mathrm{IV}}(R_s,\alpha)\cos(v\alpha)\mathrm{d}\alpha = \frac{-v}{\mu_0 R_s}\left(A_3^v - B_3^v\left(\frac{R_m}{R_s}\right)^v\right) \\ \frac{1}{\pi}\int_{\alpha_k-\frac{bc\alpha}{2}}^{\alpha_k+\frac{bc\alpha}{2}} H_{\alpha\mathrm{IV}}(R_s,\alpha)\sin(v\alpha)\,\mathrm{d}\alpha = \frac{-v}{\mu_0 R_s}\left(C_3^v - D_3^v\left(\frac{R_m}{R_3}\right)^v\right) \end{cases}. \tag{40}$$

After substituting the expressions of the vector magnetic potential of the two subdomains, Eq. (16) and Eq. (20), into Eq. (38), and expanding the vector magnetic potential of the air gap subdomain (Subdomain III) along the sector auxiliary opening slot subdomain (Subdomain IV) by Fourier series, the following can be obtained:

$$\begin{cases} \frac{2}{b_{ca}}\int_{\alpha_k-\frac{bc\alpha}{2}}^{\alpha_k+\frac{bc\alpha}{2}} A_{z\mathrm{III}}(R_s,\alpha)\cos\left(F_\chi\left(\alpha-\alpha_k+\frac{b_{ca}}{2}\right)\right)\mathrm{d}\alpha = C_4^\chi\left(\frac{R_s}{R_e}\right)^{\frac{\chi\pi}{bca}} + D_4^\chi \\ \frac{1}{O}\int_{\alpha_k-\frac{bc\alpha}{2}}^{\alpha_k+\frac{bc\alpha}{2}} A_{z\mathrm{III}}(R_s,\alpha)\mathrm{d}\alpha = A_4^0 \end{cases}. \tag{41}$$

This paper has been accepted for publication in the AEE journal. This is the version, which has not been fully edited and content may change prior to final publication.
Citation information: DOI 10.24425/aee.2026.3545

3.4. Interface between Subdomain III and Subdomain V

At the interface between the air gap subdomain and the stator slot opening subdomain, that is, at the radius of the inner surface of the stator, namely at $r = R_s$, the vector magnetic potential is continuous across the interface:

$$A_{z\mathrm{III}}|_{r=R_s} - A_{zV}|_{r=R_s} = 0,\quad \theta_j - \frac{b_{oa}}{2} \le \alpha \le \theta_j + \frac{b_{oa}}{2}, \tag{42}$$

$$H_{\alpha\mathrm{III}}|_{r=R_s} - H_{\alpha V}|_{r=R_s} = 0,\quad \theta_j - \frac{b_{oa}}{2} \le \alpha \le \theta_j + \frac{b_{oa}}{2}, \tag{43}$$

After substituting the expressions of the tangential magnetic field intensity of the two subdomains, Eq. (17) and Eq. (25), into Eq. (43), and unifying the tangential component of the magnetic field intensity in the stator slot opening (Subdomain V) to the interval $[0,\ 2\pi]$ by Fourier transform, the following can be obtained:

$$\begin{cases} \frac{1}{\pi}\int_{\theta_j-\frac{b_{o\alpha}}{2}}^{\theta_j+\frac{b_{o\alpha}}{2}} H_{\alpha \mathrm{V}}(R_s,\alpha)\sin(v\alpha)\mathrm{d}\alpha = \frac{-v}{\mu_0 R_s}\left(C_3^v - D_3^v\left(\frac{R_s}{R_m}\right)^{-v}\right) \\ \frac{1}{\pi}\int_{\theta_j-\frac{b_{o\alpha}}{2}}^{\theta_j+\frac{b_{o\alpha}}{2}} H_{\alpha \mathrm{V}}(R_s,\alpha)\cos(v\alpha)\,\mathrm{d}\alpha = \frac{-v}{\mu_0 R_s}\left(A_3^v - B_3^v\left(\frac{R_s}{R_m}\right)^{-v}\right) \end{cases}. \tag{44}$$

After substituting the expressions of the vector magnetic potential of the two subdomains, Eq. (16) and Eq. (24), into Eq. (42), and expanding the vector magnetic potential of the air gap (Subdomain III) along the stator slot opening (Subdomain V) by Fourier series, the following can be obtained:

$$\begin{cases} \frac{2}{b_{o\alpha}}\int_{\theta_j-\frac{b_{o\alpha}}{2}}^{\theta_j+\frac{b_{o\alpha}}{2}} A_{z\mathrm{III}}(R_s,\alpha)\cos\left(F_k\left(\alpha-\theta_j+\frac{b_{oa}}{2}\right)\right)\mathrm{d}\alpha = C_5^k\left(\frac{R_s}{R_t}\right)^{\frac{k\pi}{b_{o\alpha}}} + D_5^k \\ \frac{1}{b_{o\alpha}}\int_{\theta_j-\frac{b_{o\alpha}}{2}}^{\theta_j+\frac{b_{o\alpha}}{2}} A_{z\mathrm{III}}(R_s,\alpha)\mathrm{d}\alpha = B_5^0 \ln R_s + A_5^0 \end{cases}. \tag{45}$$

3.5. Interface between Subdomain V and Subdomain VI

At the interface between the stator slot opening subdomain and the stator slot subdomain, that is, at the radius of the stator slot opening, namely $r = R_t$, the vector magnetic potential is also continuous across the interface:

$$A_{z\mathrm{VI}}|_{r=R_t} - A_{zV}|_{r=R_t} = 0,\quad \theta_j - \frac{b_{oa}}{2} \le \alpha \le \theta_j + \frac{b_{oa}}{2}, \tag{46}$$

$$H_{z\mathrm{VI}}|_{r=R_t} - H_{zV}|_{r=R_t} = 0,\quad \theta_j - \frac{b_{oa}}{2} \le \alpha \le \theta_j + \frac{b_{oa}}{2}. \tag{47}$$

After substituting the expressions of the tangential magnetic field intensity of the two subdomains, Eq. (25) and Eq. (29), into Eq. (47), and unifying the tangential component of the magnetic field intensity in the stator slot opening (Subdomain V) to the interval $\left[\theta_j - \frac{b_{sa}}{2}, \theta_j + \frac{b_{sa}}{2}\right]$ by Fourier transform, the following can be obtained:

$$\begin{cases} \frac{2}{b_{s\alpha}} \int_{\theta_j - \frac{b_{o\alpha}}{2}}^{\theta_j + \frac{b_{o\alpha}}{2}} H_{\alpha V}(R_s, \alpha) \cos\left(F_\gamma \left(\alpha - \theta_j + \frac{b_{sa}}{2}\right)\right) \mathrm{d}\alpha = \frac{-F_\gamma B_6^\gamma}{\mu_0 R_t} \left[\left(\frac{R_{sh}}{R_t}\right)^{-\frac{2\gamma\pi}{b_{o\alpha}}} - 1\right] \\ \frac{1}{b_{s\alpha}} \int_{\theta_j - \frac{b_{o\alpha}}{2}}^{\theta_j + \frac{b_{o\alpha}}{2}} H_{\alpha V}(R_t, \alpha) \mathrm{d}a = 0 \end{cases} . \quad (45)$$

After substituting the expressions of the vector magnetic potential of the two subdomains, Eq. (24) and Eq. (28), into Eq. (46), and expanding the vector magnetic potential of the stator slot (Subdomain VI) along the stator slot opening (Subdomain V) by Fourier series, the following can be obtained:

$$\begin{cases} \frac{2}{b_{o\alpha}} \int_{\theta_j - \frac{b_{o\alpha}}{2}}^{\theta_j + \frac{b_{o\alpha}}{2}} A_{z\mathrm{VI}}(R_t, \alpha) \cos\left(F_k \left(\alpha - \theta_j + \frac{b_{oa}}{2}\right)\right) \mathrm{d}\alpha = C_5^k + D_5^k \left(\frac{R_s}{R_t}\right)^{\frac{k\pi}{b_{o\alpha}}} \\ \frac{1}{b_{o\alpha}} \int_{\theta_j - \frac{b_{o\alpha}}{2}}^{\theta_j + \frac{b_{o\alpha}}{2}} A_{z\mathrm{VI}}(R_t, \alpha) \mathrm{d}a = A_5^0 + B_5^0 \ln R_t \end{cases} . \quad (49)$$

By combining the above equations, namely equations (32), (33), (36), (37), (40), (41), (44), (45), and (48), (49), into a unified system, a closed linear system of equations is obtained and solved to determine the harmonic coefficients in all subdomains, thereby yielding the analytical distributions of the vector magnetic potential and magnetic flux density in each subdomain. In the analytical calculation model, the expressions of the radial and tangential components of the magnetic flux density in the air gap subdomain are:

$$\begin{cases} B_{3r} = \sum_{v=1}^{\infty} \frac{-v}{r} \left[A_3^v \left(\frac{r}{R_s}\right)^v + B_3^v \left(\frac{r}{R_m}\right)^{-v}\right] \sin(v\alpha) + \sum_{v=1}^{\infty} \frac{v}{r} \left[C_3^v \left(\frac{r}{R_s}\right)^v + D_3^v \left(\frac{r}{R_m}\right)^{-v}\right] \cos(v\alpha) \\ B_{3r} = \sum_{v=1}^{\infty} \frac{-v}{r} \left[A_3^v \left(\frac{r}{R_s}\right)^v - B_3^v \left(\frac{r}{R_m}\right)^{-v}\right] \cos(v\alpha) - \sum_{v=1}^{\infty} \frac{v}{r} \left[C_3^v \left(\frac{r}{R_s}\right)^v - D_3^v \left(\frac{r}{R_m}\right)^{-v}\right] \sin(v\alpha) \end{cases}, \quad (50)$$

4. Finite-element verification and analysis

4.1. Finite-element verification of the analytical method

To verify the accuracy of the analytical model for the no-load air gap magnetic field of the slotted motor, the FEM is used to solve the air gap magnetic field, and the results are compared with the analytical results. The waveform and harmonic spectrum comparisons of the radial air gap flux density are shown in Fig. 4.

This paper has been accepted for publication in the AEE journal. This is the version, which has not been fully edited and content may change prior to final publication.
Citation information: DOI 10.24425/aee.2026.3545

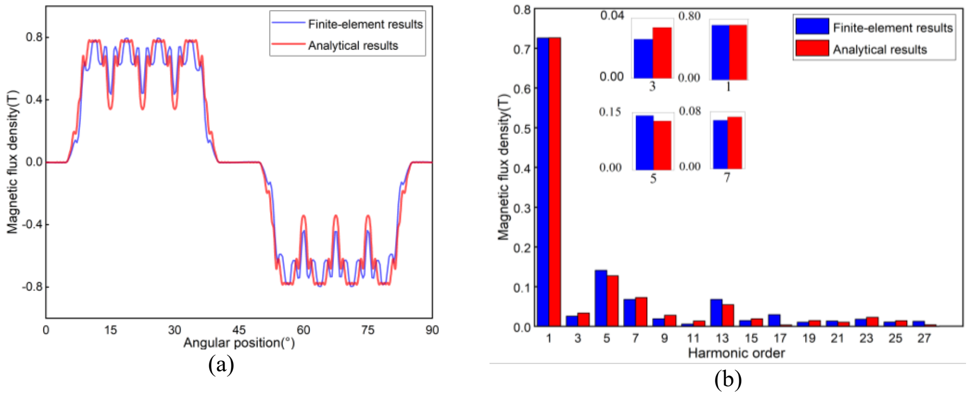

Fig. 4. Waveform and harmonic spectrum comparisons of the radial air gap flux density: waveform comparison of radial flux density (a); harmonic spectrum comparison of radial flux density (b)

As can be seen from Fig. 4(a), the analytical results of the radial air gap flux density agree well with the finite-element results as a whole, and the waveform variation trends and main characteristic points of the two are basically consistent, with only slight deviations at the slot opening. As can be seen from Fig. 4(b), the errors in the fundamental and main harmonic amplitudes between the analytical results and the finite-element results are small, and the difference in the fundamental amplitude is only 0.024%.

The waveform and harmonic spectrum comparisons of the tangential air gap flux density are shown in Fig. 5.

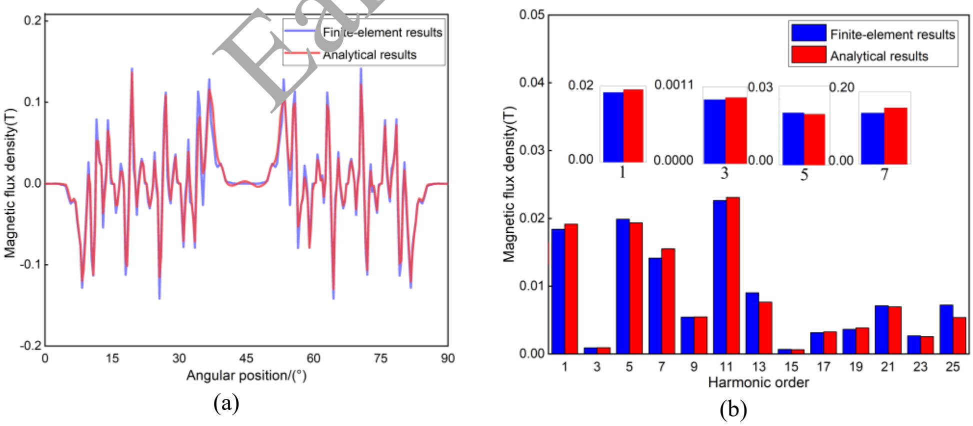

Fig. 5. Waveform and harmonic spectrum comparisons of the tangential air gap flux density: waveform comparison of tangential flux density (a); harmonic spectrum comparison of tangential flux density (b)

As can be seen from Fig. 5(a), the analytical results of the tangential air gap flux density are generally consistent with the finite-element results, and only slight differences exist at several

This paper has been accepted for publication in the AEE journal. This is the version, which has not been fully edited and content may change prior to final publication.
Citation information: DOI 10.24425/aee.2026.3545

individual peaks and valleys. As can be seen from Fig. 5(b), the errors in the fundamental and main harmonic amplitudes of the two are small, and the error of the fundamental amplitude is 2.5%.

4.2. Performance comparison of the motor before and after slotting

The FEM is used to verify the effect of the auxiliary slots on improving the electromagnetic performance and output performance of the motor. The waveform and harmonic spectrum comparisons of the air gap flux density of the motor before and after slotting are shown in Fig. 6.

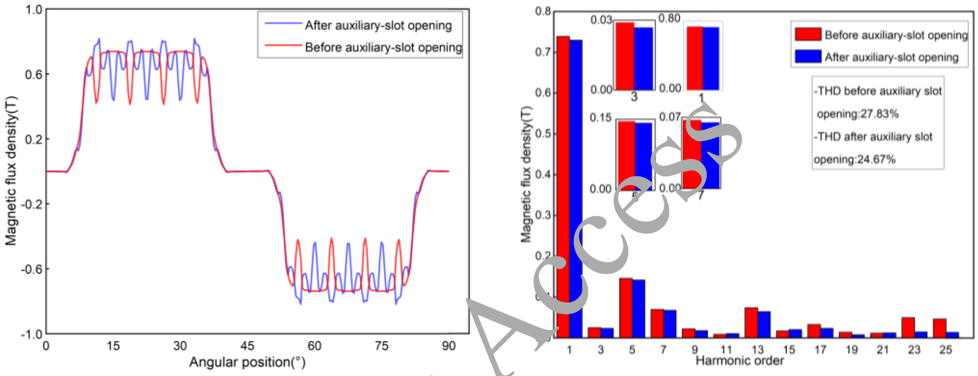

Fig. 6. Waveform and harmonic spectrum comparisons of the air gap flux density of the motor before and after slotting: waveform comparison of air gap flux density (a); harmonic spectrum comparison of air gap flux density (b)

As can be seen from Fig. 6(a), the introduction of auxiliary slots increases the amplitude of the air gap flux density and effectively improves the sinusoidal shape of the waveform. As can be seen from Fig. 6(b), the amplitudes of the dominant harmonic components of the air gap flux density are reduced after slotting, and the waveform distortion rate decreases from 27.83% to 24.67%, with a reduction of 11.4%. Therefore, the auxiliary slot design optimizes the air gap magnetic-field distribution and improves the quality of the main air gap magnetic field.

The comparisons of the cogging torque and the output torque under rated operating conditions of the motor before and after slotting are shown in Fig. 7.

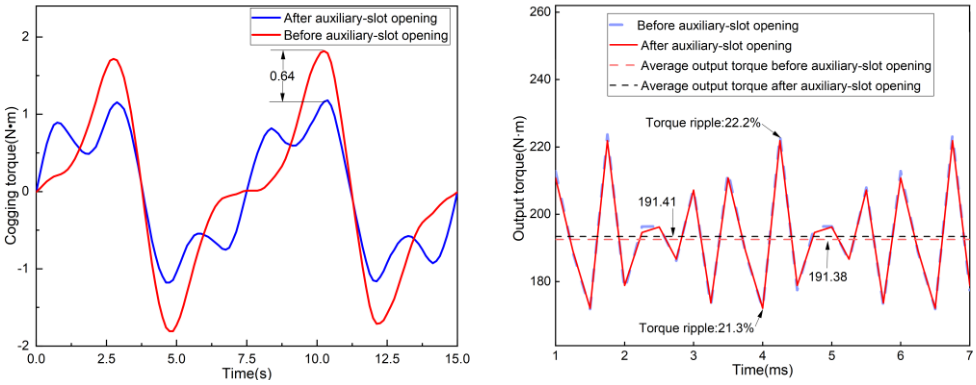

Fig. 7. Comparison of the cogging torque and output torque before and after slotting: comparison of cogging torque (a); comparison of output torque (b)

As can be seen from Fig. 7(a), after slotting, the peak cogging torque of the motor decreases from 1.82 N·m to 1.18 N·m, with a reduction of 35%. This indicates that the auxiliary-slot design effectively suppresses the cogging effect. As can be seen from Fig. 7(b), under rated operating conditions, the average output torque of the motor after slotting increases, and the torque ripple decreases from 22.2% to 21.3%. The output torque becomes more stable, and the operating performance is improved. These improvements are of great significance for smooth operation, overall motor performance, and subsequent structural optimization.

5. Conclusions

This paper takes a Toyota Prius V-type IPMSM with stator auxiliary slots as the research object and establishes a magnetic field analytical model of the IPMSM with stator slotting based on the exact subdomain method. The stator auxiliary slot parameters are incorporated into the subdomain model, and based on the conservation principles of the electromagnetic parameters of the PM material, the interior V-type PM poles are equivalently transformed into U-type poles with regular boundaries, thereby improving the magnetic field modeling accuracy of the motor. The accuracy of the analytical model is verified by the FEM. The analytical results are in good agreement with the finite-element results in terms of the variation trends of the radial and tangential air gap flux density waveforms, and the errors of the fundamental amplitudes are only 0.024% and 2.5%, respectively. The electromagnetic performance and output performance of the motor before and after slotting are compared by the FEM. The results show that, after slotting, the air gap flux density waveform of the motor is effectively improved, the cogging torque is effectively reduced with its peak value decreased by about 35%, the average output torque is increased, the torque ripple is reduced, and the overall output performance is improved.

This paper has been accepted for publication in the AEE journal. This is the version, which has not been fully edited and content may change prior to final publication.
Citation information: DOI 10.24425/aee.2026.3545

Acknowledgements

This work was supported by the National Natural Science Foundation of China under Grant 52505269, the Shandong Provincial Natural Science Foundation under Grant ZR2023QE010, and the Shandong Provincial Natural Science Foundation under Grant ZR2025MS914.

References

[1] Vyas D., Morawiec M., Ayana T., Wogi L., Guziński J., *Active flux based adaptive and non-adaptive observer for sensorless interior permanent magnet synchronous machine drive*, Archives of Electrical Engineering, vol. 73, no. 3, pp. 799–815 (2024), DOI: 10.24425/aee.2024.150896.
[2] Koc M., Özçiflikçi O.E., *Precise torque control for interior mounted permanent magnet synchronous motors with recursive least squares algorithm based parameter estimations*, Engineering Science and Technology, an International Journal, vol. 34, 101087 (2022), DOI: 10.1016/j.jestch.2021.101087.
[3] Moon J.H., Kang D.W., *Torque ripple and cogging torque reduction method of IPMSM using asymmetric shoe of stator and notch in stator*, Journal of Electrical Engineering & Technology, vol. 17, no. 6, pp. 3465–3471 (2022), DOI: 10.1007/s42835-022-01266-1.
[4] Zwolnik T., Opach S., Cyganik Ł., Jarek T., Szekeres V., *Design methods for limiting rotor losses in a fractional slot PMSM motor with high power density*, Archives of Electrical Engineering, vol. 71, no. 4, pp. 963–979 (2022), DOI: 10.24425/aee.2022.142119.
[5] Huang C., Jia R.S., Chen B.B., Zhang M.L., Chen H.J., Wang Y.C., Mao J.F., *Research on cogging torque reduction based on multi-parameter optimization of auxiliary slots and pole-arc coefficient*, Journal of Electrical Engineering & Technology, vol. 20, no. 3, pp. 1439–1449 (2025), DOI: 10.1007/s42835-024-02058-5.
[6] Ji S.W., Li Y.K., Ou H.Y., Tian W.L., *Design principles and calculation criteria for skewed notches in PM motors*, Energies, vol. 16, no. 9, 3783 (2023), DOI: 10.3390/en16093783.
[7] Cui Z.S., Zhou Y.Z., Zhou Y.H., *Analytical calculation of magnetic field of dual-winding bearingless flux-switching permanent magnet motors based on improved subdomain model*, Electric Machines and Control, vol. 26, no. 3, pp. 66–77 (2022), DOI: 10.15938/j.emc.2022.03.008.
[8] Sheikh-Ghalavand B., Vaez-Zadeh S., Hassanpour Isfahani A., *An improved magnetic equivalent circuit model for iron-core linear permanent-magnet synchronous motors*, IEEE Transactions on Magnetics, vol. 46, no. 1, pp. 112–120 (2010), DOI: 10.1109/TMAG.2009.2030674.
[9] Asfirane S., Hlioui S., Amara Y., De La Barriere O., Barakat G., Gabsi M., *Global quantities computation using mesh-based generated reluctance networks*, IEEE Transactions on Magnetics, vol. 54, no. 11, 7002304 (2018), DOI: 10.1109/TMAG.2018.2829155.
[10] Zeng L.Z., Chen X.D., Amara Y., Li X.Q., Jiang W., Luo X., *A Thrust Force Analysis Method for Permanent Magnet Linear Motor Using Schwarz-Christoffel Mapping and Considering Slotting Effect, End Effect, and Magnet Shape*, IEEE Transactions on Magnetics, vol. 51, no. 9, 8107609 (2015), DOI: 10.1109/TMAG.2015.2432151.
[11] Zhang H.S., Fan M.W., Qiao J., He X.J., Yang M.L., Tuo J.Y., *Analytical prediction of electromagnetic performance for surface-embedded permanent magnet in-wheel machines considering iron's nonlinearity*, Scientific Reports, vol. 14, no. 1, 26353 (2024), DOI: 10.1038/s41598-024-77261-5.
[12] Tiang T.L., Ishak D., Jamil M.K.M., *Complete subdomain model for surface-mounted permanent magnet machines*, 2014 IEEE Conference on Energy Conversion (CENCON 2014), Johor Bahru, Malaysia, pp. 140–145 (2014).
[13] Xing Z.Z., Wang X.H., Zhao W.L., *Design and Analysis of Basic Model of High-speed Surface-mounted Permanent Magnet Synchronous Motors Based on Subdomain Method*, Journal of Electrical Engineering & Technology, vol. 18, pp. 3635–3646 (2023), DOI: 10.1007/s42835-023-01449-4.

[14] Yu Z.Y., Li Y., Jing Y.T., Du J.M., Wang J., *An improved subdomain model for magnetic field calculation of SPMSM considering no-load leakage flux*, Journal of Electrical Engineering & Technology, vol. 15, no. 6, pp. 2651–2660 (2020), DOI: 10.1007/s42835-020-00541-3.

[15] Zhang H.S., Yang M.L., Zhang Y., Tuo J.Y., Luo S., Xu J., *Analytical Calculation of Surface-Inset PM In-Wheel Motors and Reduction of Torque Ripple*, IEEE Transactions on Magnetics, vol. 57, no. 1, 8100211 (2021), DOI: 10.1109/TMAG.2020.3034882.

[16] Rahideh A., Korakianitis T., *Analytical magnetic field calculation of slotted brushless permanent-magnet machines with surface inset magnets*, IEEE Transactions on Magnetics, vol. 48, no. 10, pp. 2633–2649 (2012), DOI: 10.1109/TMAG.2012.2200691.

[17] Zhang Z., Xia C.L., Wang H.M., Shi T.N., *Analytical field calculation and analysis of surface inset permanent magnet machines with high saliency ratio*, IEEE Transactions on Magnetics, vol. 52, no. 12, 8108612 (2016), DOI: 10.1109/TMAG.2016.2599147.

[18] Xu L., Zhang C., Zhu X.Y., Lin M.Y., Zheng S.Y., *Indirect Analytical Modeling and Analysis of V-Shaped Interior PM Synchronous Machine*, IEEE Access, vol. 7, pp. 173786–173795 (2019), DOI: 10.1109/ACCESS.2019.2956764.

[19] Wu P.F., Sun Y.H., *An improved subdomain method for air gap flux density of interior permanent magnet machines based on rotor reconstruction and flux equivalence*, IET Electric Power Applications, vol. 17, no. 11, pp. 1447–1458 (2023), DOI: 10.1049/elp2.12355.

[20] Ren J., Sun F.C., Wang A.D., Li M., Xu J.Y., *Analytical prediction of the open-circuit magnetic field for the V-shaped interior PM machine by the improved subdomain method*, IET Electric Power Applications, vol. 18, no. 10, pp. 1359–1369 (2024), DOI: 10.1049/elp2.12484.

[21] Zhou H., Wang X.H., Zhao W.L., Xing Z.Z., Li X., *Magnetic field calculation of the U-shaped interior permanent-magnet synchronous machine considering the parallel magnetization and bridge saturation*, IEEE Transactions on Industrial Electronics, vol. 71, no. 10, pp. 11817–11828 (2024), DOI: 10.1109/TIE.2024.3349526.

[22] Liu F., Wang X.H., Wei H.Y., Xiong L.X., Zhang X., *Prediction of electromagnetic performance for IPMSM based on improved analytical model considering saturation effects*, IEEE Transactions on Transportation Electrification, vol. 10, no. 1, pp. 1128–1144 (2024), DOI: 10.1109/TTE.2023.3260968.

[23] Geng H.H., Zhang X.Y., Yan S.L., Zhang Y.F., Wang L., Han Y.T., Wang W., *Magnetic field analysis of an inner-mounted permanent magnet synchronous motor for new energy vehicles*, Energies, vol. 15, no. 11, 4074 (2022), DOI: 10.3390/en15114074.

[24] Hao X.H., Cai X., Nie X.L., *Analytical computation of magnetic field distribution in double-stator hybrid-excitation vernier motor based on an accurate subdomain model*, Advances in Mechanical Engineering, vol. 16, no. 5, pp. 1–13 (2024), DOI: 10.1177/16878132241256026.

[25] Liu F., Wang X.H., Wei H.Y., *Fast magnetic field prediction based on hybrid subdomain method and multiobjective optimization design for interior permanent magnet synchronous machines*, IEEE Transactions on Energy Conversion, vol. 38, no. 3, pp. 2045–2060 (2023), DOI: 10.1109/TEC.2023.3260109.

[26] An Y.S., Ma C.G., Zhang N., Guo Y., Degano M., Gerada C., Li Q.Y., Zhou S.S., *Open-circuit air-gap magnetic field calculation of interior permanent magnet synchronous motor with V-shaped segmented skewed poles using hybrid analytical method*, IEEE Transactions on Magnetics, vol. 57, no. 12, 8108309 (2021), DOI: 10.1109/TMAG.2021.3118222.

[27] Zhu M.C., Wu L.J., Wang D., Fang Y.T., Tan P., *Analytical prediction of electromagnetic performance of dual-stator consequent-pole PM machines based on subdomain model accounting for tooth-tips*, COMPEL - The International Journal for Computation and Mathematics in Electrical and Electronic Engineering, vol. 40, no. 3, pp. 289–308 (2021), DOI: 10.1108/COMPEL-01-2020-0063.

[28] Pourahmadi-Nakhli M., Kouhanjani M.J., Jafari F., Najibi S., *Analytical design of Spoke Internal Permanent Magnet machines using polar-consistent approximation of cubic subdomains*, Archives of Electrical Engineering, vol. 73, no. 4, pp. 907–926 (2024), DOI: 10.24425/aee.2024.152102.